Article

Optimizing Picene Molecular Assembling by Supersonic Molecular Beam Deposition

Stefano Gottardi,[†,#] Tullio Toccoli,*[,†] Salvatore Iannotta,[†] Paolo Bettotti,[‡] Antonio Cassinese,[§] Mario Barra,[§] Laura Ricciotti,[∥] and Yoshihiro Kubozono[⊥]

[†]IMEM-CNR-FBK Division of Trento, Via alla Cascata 56/C, I-38123 Povo, Italy

[‡]Nanoscience Laboratory, Department of Physics, University of Trento, Via Sommarive 14, I-38123 Povo Trento, Italy

[§]CNR-SPIN and Department of Physics Science, University of Naples "Federico II", P.le Tecchio 80, 80125, Naples, Italy

[∥]Department of Chemistry, University of Naples "Federico II", Via Cinthia, I-80126 Naples, Italy

[⊥]Research Laboratory for Surface Science, Okayama University, Okayama 700-8530, Japan

ABSTRACT: Here we report an investigation of the growth of picene by supersonic molecular beam deposition on thermal silicon oxide and on a self-assembled monolayer of hexamethyldisiloxane (HMDS). In both cases film morphology shows a structure with very sharp island edges and well-separated islands which size and height depend on the deposition conditions. Picene films growth on bare silicon covered with hydrophobic HDMS shows islands characterized by large regular crystallites of several micrometers; on the other hand, films growth on silicon oxide shows smaller and thicker islands. We analyzed the details of the growth model and describe it as a balancing mechanism involving the weak interaction between molecules and surface and the strong picene—picene interaction that leads to a different Schwoebel—Ehrlich barrier in the first layer with respect to the successive one. Finally, we study the charge transport properties of these films by fabricating field-effect transistors devices in both top and bottom contact configuration. We notice that substrate influences the electrical properties of the device and we obtained a maximum mobility value of 1.2 cm^2 V^{-1} s^{-1} measured on top contact devices in air.
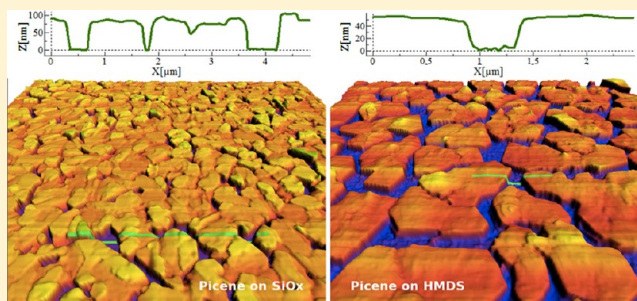
1. INTRODUCTION

Picene was revealed recently to be a very interesting molecule for organic electronics, since it was successfully applied to realize the active channels of field-effect transistors able to work in ambient conditions and even in oxygen atmosphere.[1,2] Moreover, it was recently demonstrated that if intercalated with alkali metals, picene exhibits superconductivity at 18 K, becoming the first superconducting hydrocarbon.[3,4] This discovery renewed the interest in the field of organic superconductors, and superconductivity was recently demonstrated also in other alkali metal-intercalated molecular solids based on polycyclic aromatic hydrocarbons, such as phenanthrene[4,5] (T_c = 5−6 K) and coronene[4] (T_c = 15 K).

These possibilities stimulate an intense research activity on these compounds from both theoretical and experimental points of view. So far, however, very little is known about the self-assembling properties of picene molecules, and no report is yet available to optimize deposition conditions that ensure the growth of high quality films. This is a fundamental step to improve the electronic and optoelectronic properties of these materials for future device applications.

It is well-known that controlling the energy of the molecules impinging the surface can optimize the molecular assembling.[6] Indeed, the supersonic molecular beam deposition (SuMBD)

technique has been used fruitfully to overcome some limitation in organic films growth by controlling parameters that other techniques cannot master.[6,7] In this work, we use the high energy provided to the molecules by SuMBD to study picene thin films growth with the aim of improving thin film morphology and structure. While molecule—molecule and molecule—substrate interactions shape the adsorption potential of the surface, the minimization of the surface free energy is not always ensured during the nonequilibrium process of thin film growth. Better minimization of the surface free energy can be favored by modifying the precursor state of the molecules that impinge the surface.[8] A good choice of substrate, together with sufficient energy available for the molecules on the surface, gives in general the best improvement of the film morphology and crystals size.[8] At the same time, by observing the film morphology, we can gain information about the particular molecular assembling processes involved, and we can thus optimize the formation of high-quality crystalline phase.

Here, picene growth is studied by atomic force microscopy (AFM) and ex-situ X-ray diffraction (XRD). We considered two
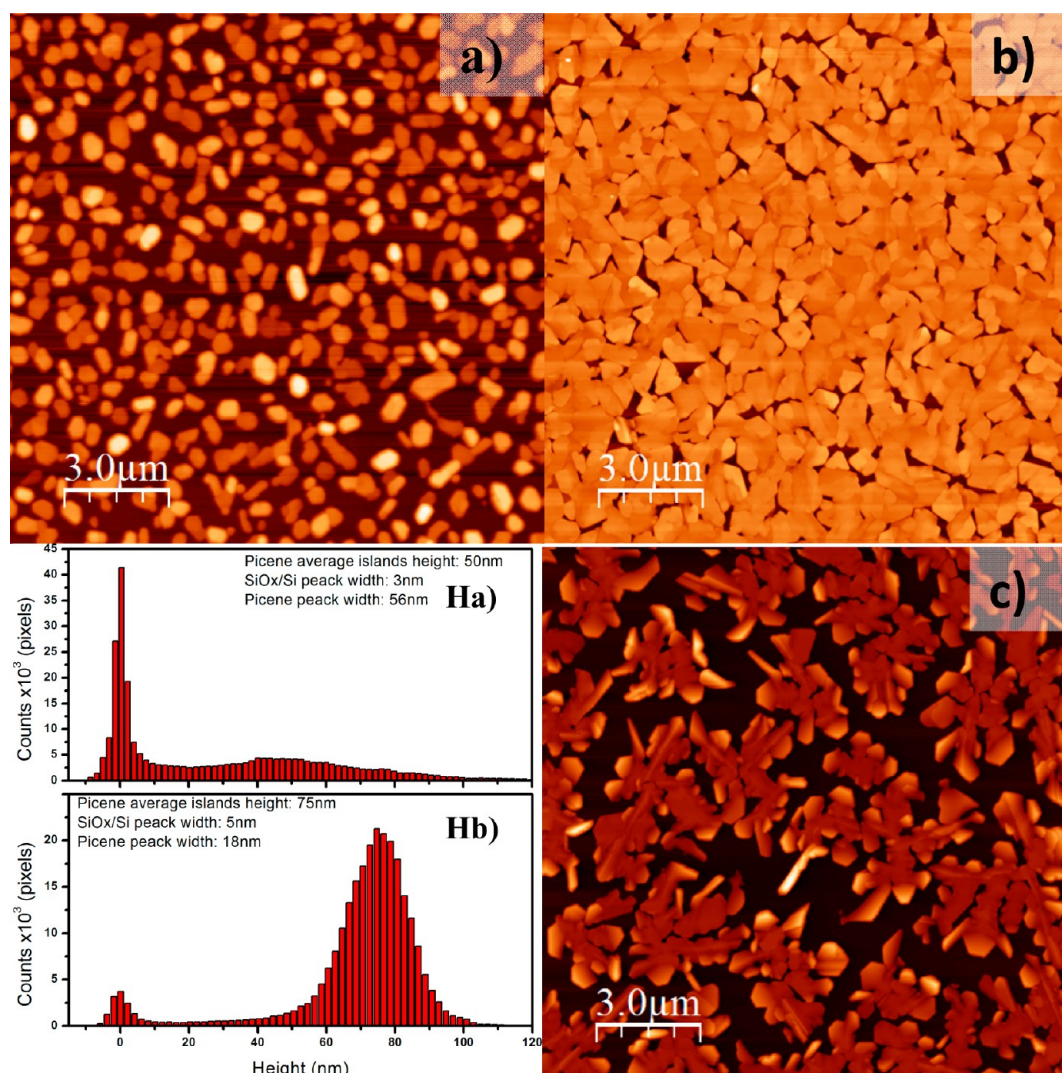
Figure 1. AFM micrographs of picene films grown by SuMBD on 50 nm thermal silicon oxide on silicon. (a) Typical growth obtained using a rate of 0.25 nm/min for a deposition time of 150 min. The histogram Ha shows the islands height distribution. The average height of picene island is about 50 nm. (b) Same condition of growth but for a deposition time of 300 min. The histogram Hb shows the islands height distribution that after the coalescence becomes narrower. (c) Typical growth for defect assisted nucleation obtained at extremely low growth rate.

different surfaces. In a first set of experiments, we deposited picene on SiO_x/Si. Our results are compared with those achieved by Kubozono group using a high-vacuum (10^{-8} mbar) thermal deposition technique. We focused our studies on the growth of picene films using a kinetic energy of the impinging molecules of about 7.0 eV, obtained seeding the molecules in a supersonic He jet. Such highly energetic conditions have been shown to be the optimal to improve the growth processes in the case of several organic molecules such as pentacene and oligothiophenes.[8,9] A second set of samples was grown on a self-assembled monolayer (SAM) of HMDS to compare the islands growth on surfaces with different wettability. Finally, we report the electrical characterization of field-effect transistor devices (FET) in bottom- and top-contact configuration. The results are then compared with state-of-the-art ones.[4]

2. EXPERIMENTAL SECTION

2.1. Substrate Preparation (Silicon Oxide). The depositions were done on 50 nm thick thermal SiO_x/Si^{2+} (purchased from Jocam Srl) with a surface root-mean-square roughness of about 0.2 nm. Silicon substrates were cleaved into 10×10 mm^2

pieces and cleaned by sonication in acetone for 10 min. A second cleaning step was done in iso-2-propanol in ultrasonic bath for 10 min. Samples were then dried with N_2 (99.995%). After the cleaning process, the contact angle, determined by the sessile drop method using deionized water, measures $60 \pm 2°$. The substrate was outgassed at 250 °C in ultrahigh vacuum (UHV) for 9 h before the deposition. The deposition was made at room temperature (25 °C).

2.2. HMDS. The bare silicon substrates were cleaned by immersion in "piranha" solution (obtained mixing equal volumes of 96% H_2SO_4 and 30% H_2O_2 solutions) at 120 °C for 15 min and then left to cool to room temperature. Subsequently, the substrates were repeatedly rinsed with bidistilled water, immersed in methanol, and sonicated for 10 min. Subsequently, substrates were repeatedly rinsed with dichloromethane and dried under N_2 flow. Freshly cleaned substrates were inserted in sealed glass vessel, several vacuum–nitrogen cycles were carried out, and HMDS (1 mL) was added with a syringe trough a rubber septum. After 4 days, the substrates were removed from the glass vessel, sonicated in both hexane and methanol for 10 min, and repeatedly rinsed with dichloromethane and dried under N_2 flow.

The self-assembled coupling layer was characterized by advancing aqueous contact angle (θ_a) measurements. The contact angles changes from 15° after the treatment with piranha to 110° for the silylated surface. This hydrophobic change in θ_a is consistent with the presence of organosilane homogeneous monolayer on the surface. Substrates were outgassed at 90 °C for 9 h in UHV.

2.3. Picene Deposition by Supersonic Molecular Beam Deposition (SuMBD). SuMBD system details can be found elsewhere.[6] The raw picene material was synthesized according the previous report from ref 1, and it was used after outgassing the evaporation cell at a temperature slightly lower than the picene sublimation temperature. We used an in-line time-of-flight mass spectrometer (ToF-MS) to check the beam purity and to control the information regarding the energetic parameters of the seeded molecular beam and its flux. To define the supersonic expansion, a pressure 2 bar of He was used to accelerate picene molecules up to the energy of 7 eV.

2.4. Atomic Force Microscopy (AFM). Topographic characterization of the films was performed by AFM microscopy in air, using a Smena SFC050 scanning head by NTMDT. Measurements were carried out in semicontact mode AFM (using NSG11 silicon cantilevers by NTMDT) and in contact mode (using CSG10 Au coated silicon cantilever by NTMDT). The detailed analysis of AFM data was performed with the WSxM software (version 5.0 Develop 1.1, Nanotec electronica).[10]

2.5. Devices Realization and Measurements. Bottom-contact bottom-gate transistors were fabricated on substrates consisting of 500 μm thick heavily doped n-type silicon layers, 200 nm thick SiO$_x$ thermally grown dielectric barrier, and interdigitated gold source-drain contacts. The utilized electrode configuration defines active channels with width (W) and length (L) of 22 mm and 40 μm, respectively.[11]

For the top-contact devices, picene films were grown on the same SiO$_x$/Si substrates, without the presence of prepatterned electrodes. In this case, both source and drain contacts were deposited by thermal evaporation of ~50 nm gold films through a shadow mask on top of the organic layers. Transistors with a channel aspect ratio W/L of 1000:100 μm (devices A), 750:75 μm (devices B), 500:50 μm (devices C), and 250:50 μm (devices D) were realized on each sample.

For all devices, the electrical characterization was performed in either air or vacuum (at 10^{-5} mbar, after 30 min of storage) using a Janis probe station. I_{DS} vs V_{GS} (drain-source current vs gate-source voltage at fixed drain-source voltages) transfer curves were recorded using a Keithley 2612A dual-channel source meter. During the measurements, the devices were kept in dark. Both mobility (μ) and threshold voltage (V_{th}) values were extracted from the transfer curves by modeling the experimental data with the standard MOSFET equation valid in the saturation regime ($|V_{GS} - V_{th}| \leq |V_{DS}|$):

$$I_{DS} = \frac{W \mu C_{ox}}{2L}(V_{GS} - V_{th})^2 \quad (1)$$

where C_{ox} is the dielectric barrier capacitance per unit area. In particular, based on this expression and assuming a uniform distribution of the drain-source current in the transistor active channels,[12] mobility was evaluated by using the relation

$$\mu_{lin} = \left(\frac{\partial \sqrt{I_{DS}}}{\partial V_{GS}}\right)^2 \frac{2L}{WC_{ox}} \quad (2)$$

According to eq 1, the threshold voltages were instead calculated from the transfer curves in saturation by estimating the V_{GS} values at which the linear fit of the square root of the I_{DS} current plotted versus V_{GS} intercepts the V_{GS} voltage axis. For all the extracted parameters, the I_{DS} curves recorded in the forward V_{GS} scans were considered.

3. RESULTS AND DISCUSSION

3.1. Morphology. Figures 1a and 1b show the film morphology for two picene films obtained with different exposure times (150 and 300 min, respectively) depositing on SiO$_x$/Si. The nominal deposition rate was about 0.25 nm min^{-1}. This low rate improves the molecules assembly and favors a single molecule adsorption process and a diffusion-mediated growth.[13] As described in detail below, we observed that picene assembly on silicon oxide surfaces is strongly dominated by molecule−molecule interactions while the interaction with this substrate is weak. Picene assembly is very different from the growth commonly obtained for the widely studied and similar pentacene molecules.[7] In fact, the AFM images evidence picene molecules that nucleate in islands developing a 3D growth that does not expand on the surface along the $a−b$ crystallographic plane. On the other hand, the growth that we observe is not a defect assisted 3D growth because thick islands with very regular shape and sharp edges are present. The morphology we obtain for picene from a pure defect-assisted growth is instead reported in Figure 1c. We observe this latter growth maintaining very low rate of molecules impinging the surface during the nucleation regime (a rate more than 100 times lower with respect to that used previously). In this condition only the most stable adsorption sites (such as surface dislocations and steps) are suitable to initiate the formation of new islands. Starting from a surface defect or impurity, many domains with different crystal orientations develop determining the formation of 3D, irregular shaped, and fractal crystals.

On the other hand, even in the typical case of a diffusion-mediated growth, we observe a quite rough morphology and not completely covered surface. While the average film thickness is 75 nm, about 1 μm^2 picene single crystals are formed but do not well interconnect to each other. The growth does not seem to follow the Stransky−Krastanov model,[14] typically observed for other organic molecules such as pentacene[7] or oligothiophenes.[15] At the same time, the islands do not show the mound expected for a classical 3D growth (Volmer−Weber).[14] To rationalize this particular growth, we assume that molecules−molecules and molecules−surface interactions are strongly unbalanced. We believe that molecules impinging either on a bare substrate or onto an already formed island show very different sticking coefficients that determine greater desorption probability from the SiO$_x$/Si than from picene islands. This adsorption model is consistent with the low maximum temperature at which picene molecules stick on the SiO$_x$/Si surface (except in the presence of defects or using very high fluxes) that we have found to be only 35 °C, while the films at this temperature are stable. The fast desorption of the molecules affects the probability of multiple scattering processes between the molecules on the surface and thus hinders the formation of stable nuclei of molecules. Figures 1Ha and 1Hb clearly show the presence of two stages in the growth: In the precoalescence stage picene nucleates into islands that develop into a very broad height distribution (Figure 1Ha); this morphology is a mark of a slow nucleation process. For this reason the growth and nucleation processes cannot be considered well-separated stages

in the thin film formation. Instead, after islands coalescence, the interislands transport of molecules drives a more homogeneous height distribution and film growth (Figure 1Hb).

This growth model can be described qualitatively considering the arrival of a picene molecule during the initial phase of the film growth. At low coverage, events of molecules impinging on an already formed island are rather rare; thus, rescattering processes are favored. With increasing the picene coverage, arriving molecules easily find stable position within already formed crystals, rescattering is thus minimized and the growth change from 3D-like to 2D-like.

We have also performed the structural characterization of the picene films by XRD. Spectra are reported in Figure 2, showing
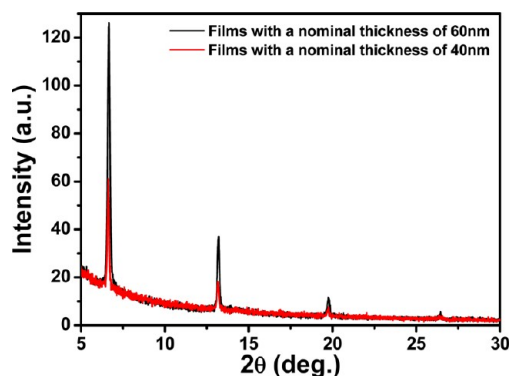

Figure 2. XRD spectra of picene films grown on SiO$_x$/Si. The spectra were collected in Bragg−Brentano geometry using a Cu anode (wavelength of 1.5406 Å). The step size is 0.05° (2Θ), and the acquisition time is 60 s/step. Different spectra belong to different film thickness.

the presence of a single crystalline phase. The peaks, assigned to the plane diffraction, give an interplane distance of about 1.3 nm, indicating that molecules are oriented with the major axes almost perpendicular with respect to the surface. This finding agrees very well with the molecular orientation observed by Kaji et al.[16]

A comparison of our results with the literature shows that the crystal size obtained in SuMBD deposited films are in general larger and thicker by a factor of 2 compared with films grown with thermal evaporation techniques.[16] To this regard, indeed, it should be remembered that the morphology of thermally evaporated picene films on SiO$_x$/Si substrates, with or without the functionalization through hydrophobic layers (i.e., HMDS or Cytop), is characterized by the presence of rounded-shaped crystalline grains displaying an average size that never exceeds 500 nm.

The considerable enhancement of the crystalline quality in the picene films deposited by the SuMBD deposition can be basically ascribed to the higher energy available for the molecules with the SuMBD deposition. The energy of the molecules could be enough to activate the incorporation of the impinging molecules directly into the molecular layer at the collision site. This process induces an overall molecular rearrangement of the island toward a more ordered configuration (a sort of localized annealing) and becomes available only if the incoming energy is large enough, as demonstrated by theoretical studies.[17] The probability of such events has been estimated to become sizable for kinetic energy larger than 2 eV in the case of pentacene molecules.[17] This incorporation could be one of the reason for the larger crystals observed in the SuMBD growth.

Another effect that is driven by the extra energy is the increasing of the mean free path of the molecules on the surface that gives rise to an increased probability for the molecules to reach a very stable site of adsorption. This increases the number of molecules available for the lateral growth of the island and is also relevant in determining the regular shape of the crystals that mainly show nearly 120° faceting. In fact, we observed that in SuMBD deposited films crystals grow with very sharp edges that are practically vertical for the AFM tip resolution, even if the height of the crystals is relevant. We ascribe this result to the combination of the effects discussed above and presence of a strong modification of the potential barrier (the Schwoebel−Ehrlich barrier[18,19]) for the interlayer molecular transport at the step edges of the picene−SiO$_x$ interface. The Schwoebel−Ehrlich barrier is the potential barrier for the interlayer molecular transport at the step edges—practically an additional potential barrier that a diffusing molecules must overcome hopping down from the upper terrace to the lower one. Nearly layer-by-layer growth on top of the crystals, with a reduced number of terraces, suggests a Schwoebel−Ehrlich barrier that is close to zero between two picene layers. This determines a very efficient interlayer mass transport inside the island. On the contrary, islands enlargement along the a−b plane is highly hindered, symptoms of a strongly increased Schwoebel−Ehrlich barrier in the first layer due to the influence of the substrate. This determines high probability of backward scattering of molecules at island edges, favors their final adsorption at terraces step sites and leads to the observed extremely high and sharp island edges.

Because the picene Schwoebel−Ehrlich barrier is strongly influenced by the substrate, we modified the growth scenario and investigated the growth mechanism onto a self-assembly monolayer of HMDS deposited on SiO$_x$/Si. In this way, we modify the molecule−substrate interaction keeping the same substrate that will be used for the fabrication of devices. The typical morphology obtained depositing on HMDS is reported in Figure 3. We observe formation of very regular crystals with an average size about 3 times larger than that found on pristine SiO$_x$/Si. Moreover islands have highly homogeneous height, even if the substrate roughness is increased (see the histogram in Figure 3). The narrow distribution of islands height evidence a different nucleation process on HMDS. The presence of a rougher surface offers many stable adsorption sites where new islands can nucleate. For this reason the nucleation process on HMDS becomes much faster than on SiO$_x$/Si, determining the very narrow crystals height distribution observed. The higher hydrophobicity of the HMDS surface modifies the Schwoebel−Ehrlich barrier. The clear evidence of a global increase in crystals size suggests that this barrier was successfully lowered by the presence of HMDS, enhancing the probability of molecular transport from picene islands to the substrate surface. We believe this to be the main reason for the overall improvement of film morphology. Despite these differences, the assembly mechanism is preserved and very high grains with negligible surface roughness and very sharp edges are present.

To better understand the growth processes is of interest to have a closer look on how molecules assemble on top of the larger crystallites grown on HMDS. Looking in detail at the islands, we can observe how molecular terraces develop on top of the crystalline domains (Figure 4a). Terraces are strongly evidenced by measuring the friction signal with lateral force microscopy (LFM) (Figure 4b). We notice that terraces edges grow with no preferred direction in contrast with the well-defined directions of the islands edges. From the LFM image is
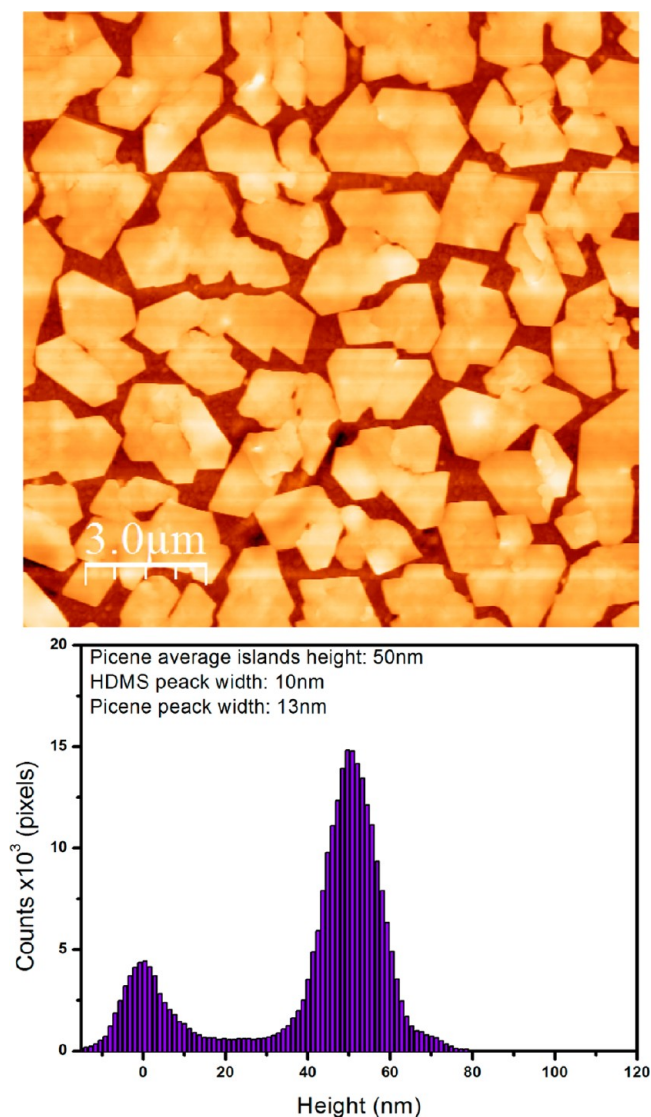
Figure 3. AFM micrograph and height histogram of a picene film grown on HMDS surface. The average height of the picene islands is 50 nm. The typical grain size is of about 4 μm^2.

clear that terraces growth stops when they reach the island edge while terraces step distance is instead very large. This is the same behavior observed on silicon oxide surfaces and confirms a small Schwoebel−Ehrlich barrier between two adjacent picene layers. On the other hand, when two islands coalesce, we observe an increase formation of screw type dislocations that affect the subsequent growth. This leads to an increased density of terraces and a larger number of defected sites (Figure 4c,d).

The interesting results obtained for picene deposited on HMDS suggest the use of this surface to realize FET devices in both top- and bottom-contact configuration. This latter is known to be more difficult to realize because of the formation of highly defected regions at the contacts−channel interface. However, by using a SAM as intermediate layer, it is possible to provide a homogeneous underlying layer for the molecules assembling also at the contact−channel interface. To this end, Figure 5a shows the growth of picene on the interface between SiO_x/Si and the bottom configuration gold contacts without presence of a SAM. Gold contacts are evidenced by the more defected growth of picene in those regions. Many elongated structures can be

noticed that influence the growth of neighboring crystals, particularly at the interface. On the other hand, the growth on HMDS shows a homogeneous interface throughout the contact edge (Figure 5b), thus reducing the height of the Schottky barrier that is often limiting the performances of these devices.

3.2. Transistor Electrical Characterization. The electrical properties of picene thin films deposited by SuMBD were analyzed fabricating field-effect transistors on both bare and HMDS-treated SiO_x/Si substrates. Nominally 100 nm thick picene films were used to ensure the percolation limit. Devices with top- and bottom-contact configurations were fabricated on both surface types. Suitable layouts for the gold electrodes were adopted for top- and bottom-contact devices, as sketched in Figures 6a and 8a, respectively.

The results of electrical characterizations agree very well with the film morphological features above-described, confirming that improved charge transport performances can be achieved in presence of a better crystalline quality of the deposited films. Indeed, while top-contact devices on bare SiO_x/Si displayed very poor performances (not shown here) with mobility values never exceeding 6×10^{-4} cm^2 V^{-1} s^{-1}, HMDS treatment of SiO_x/Si surfaces provides a mobility improvement of more than 3 orders of magnitude, reflecting the changes in the film and contact interface morphology.

To this purpose, Figures 6b and 6c show two transfer curves recorded in air and in vacuum, respectively, for the same top-contact device fabricated on HMDS-treated substrate. In the insets, the same curves are reported in semilog plots. These curves were measured in the saturation regime by applying $V_{DS} = -80$ V in air and $V_{DS} = -50$ V in vacuum. Typically, a large hysteresis was observed between the I_{DS} current detected in the forward (going from the off to the on electrical region) and the reverse scans of the V_{GS} voltage. This feature is commonly reported also for picene transistors fabricated by OMBD on HMDS-treated SiO_x/Si surfaces[20] and can be mainly ascribed to charge trapping mechanisms still active at the organic/dielectric interface rather than to the film morphology. Similar trapping processes can be invoked to justify the occurrence of bias stress phenomena in these devices, too. In general, it was reported that both these effects could be strongly reduced by using appropriate hydrophobic polymer layers (i.e., Cytop) coating the SiO_x/Si surface, as experimentally demonstrated for picene devices[20] as well as for other types of p- and n-type transistors.[21,22]

In top-contact devices, a maximum mobility value of 1.2 cm^2 V^{-1} s^{-1} was measured in air, while lower mobility, getting the largest value of 0.3 cm^2 V^{-1} s^{-1}, were detected in a vacuum. Concerning the electrical operation in air of these transistors, the on−off ratios resulted to exceed 10^5 (see the inset in Figure 6b), while a reduction by a factor between 2 and 3 was observed in vacuum, which should be mainly ascribable to the mobility lowering.

These results confirm the previously reported data on picene transistors,[1,2] where oxygen was demonstrated to play a beneficial role in affecting the charge transport properties of this compound, different from what commonly observed for other p-type materials.[23]

In particular, it was proposed that, in form of partly ionized molecules, O_2 may inhibit the action of shallow traps related to the presence of positively charged defects or impurities.[2] This effect, rather than a simple charge chemical doping, is believed to justify the enhancement of the picene charge transport properties when the material is immersed in O_2-rich atmospheres.[1]
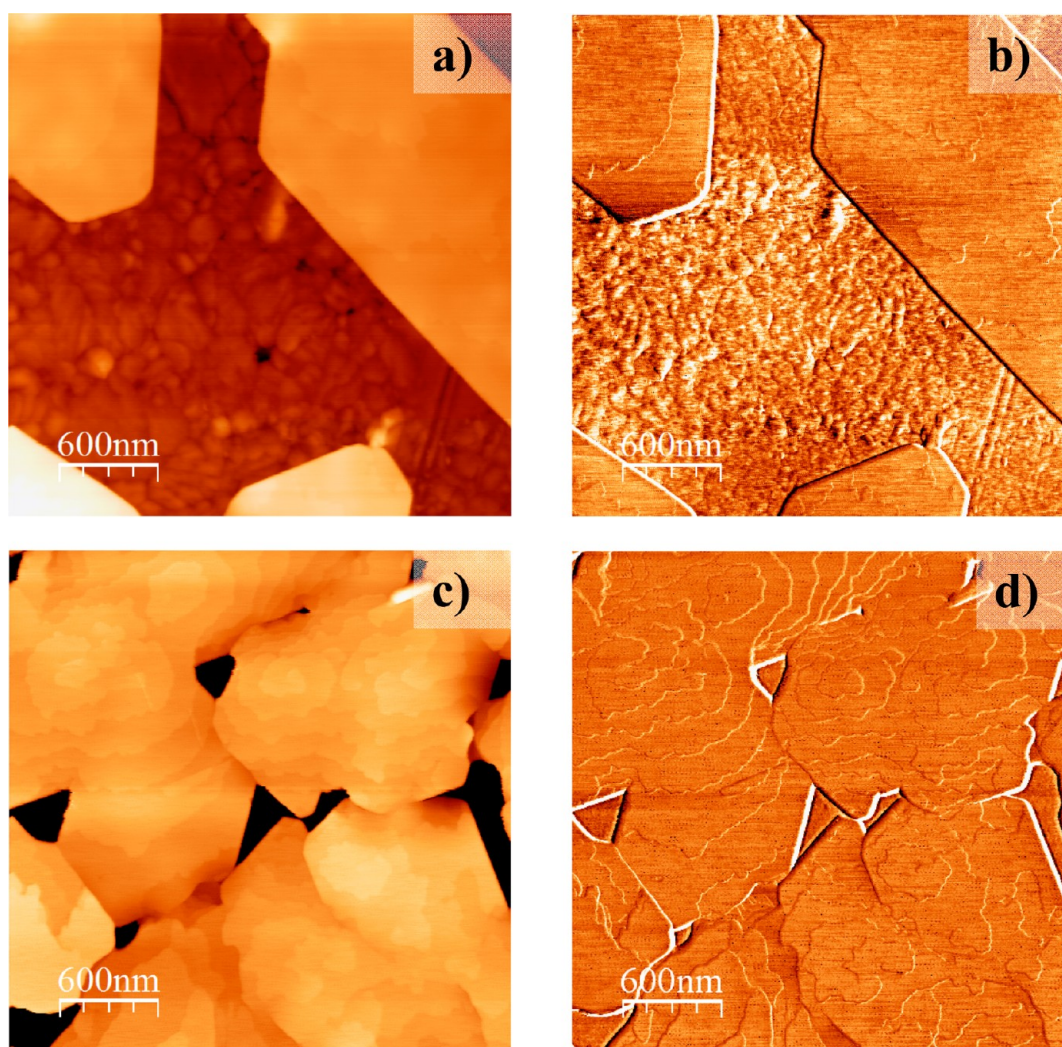
Figure 4. (a) High-resolution AFM micrograph showing the topography of a picene film grown on HMDS before the coalescence of the grains. Note the sharpness of the island edges and the crystalline aspect of the islands. (b) The corresponding LFM image of (a) evidence the molecular terraces. (c) High-resolution AFM micrograph of a picene film grown on HMDS after the coalescence of the grains. (d) The corresponding LFM image of (c). Note that at this point of the growth many dislocations start to form.
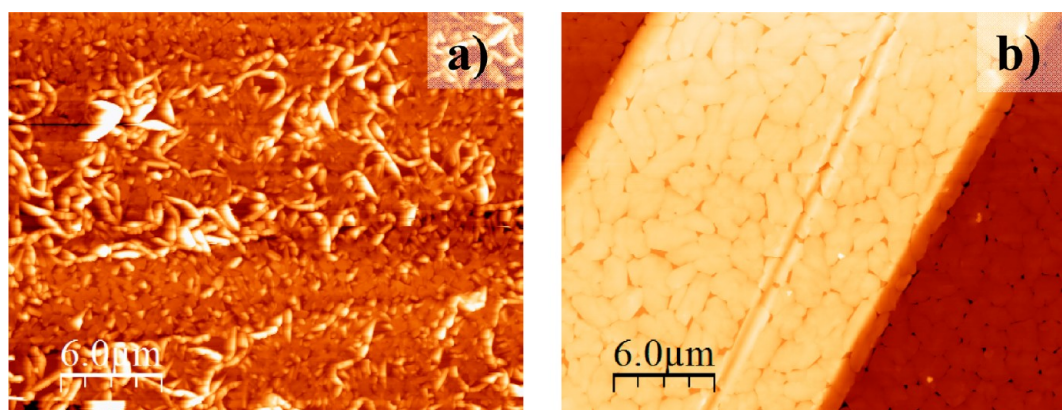
Figure 5. (a) AFM micrograph showing the typical picene growth on SiO_x/Si at the interface with Au contacts. The presence of the Au contact modifies the growth of picene crystals increasing the number of defects in particular at the interface. (b) Morphology of the picene films when a HMDS layer covers the surface and the Au contacts. The picene crystals are now very regular and grow homogeneously across the Au–SiO_x interface.

We characterized more than 30 top-contact devices fabricated on HMDS-treated surfaces and having different W/L ratios (see the Experimental Section for the geometry details) of the active channels. With the reference to the overall set of the analyzed devices, Figure 7 reports a statistical analysis focused on the values of mobility, onset voltage V_{on} (here defined as the V_{GS} voltage where the I_{DS} current starts to increase in the semilog plot), and threshold voltages V_{th} estimated in air.
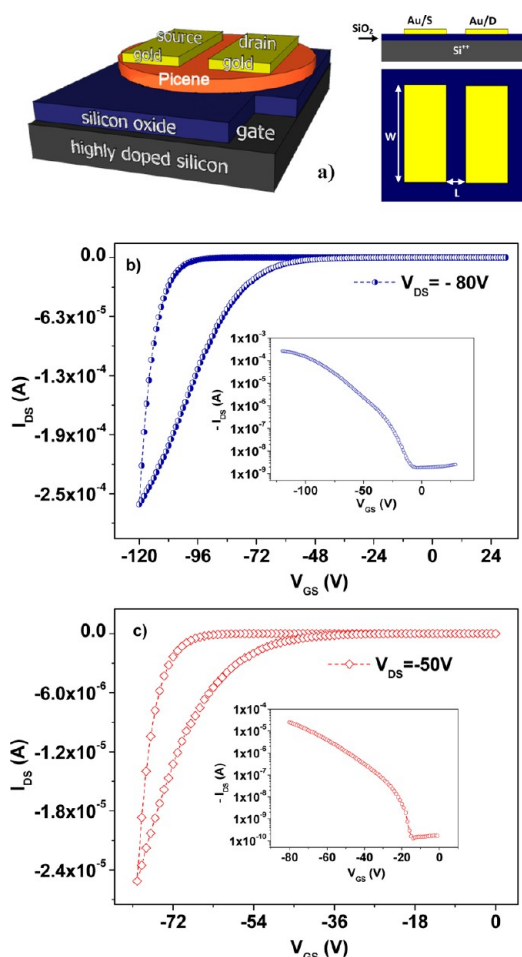
Figure 6. (a) Top-contact transistor configuration and corresponding source-drain electrode layout considered in this work. (b, c) Transfer curves in saturation measured (b) in air and (c) in vacuum for a top-contact picene transistor. The insets in (b) and (c) show the same transfer curves plotted in a semilog graph.

Figure 7. (a) Mean values of mobility, (b) onset and (c) threshold voltages estimated in air for top-contact devices having different widths (W) and lengths (L) of the active channel. For devices A, $W = 1000\ \mu$m and $L = 100\ \mu$m; for devices B, $W = 750\ \mu$m and $L = 75\ \mu$m; for devices C, $W = 500\ \mu$m and $L = 50\ \mu$m; for devices D, $W = 250\ \mu$m and $L = 50\ \mu$m. The error bars represent the standard deviations.

We can observe (see Figure 7a) that, for devices where the W/L ratio was the same (about 10), the average mobility decreased going from devices A ($\mu_{mean} = 0.78$ cm^2 V^{-1} s^{-1}) to devices C ($\mu_{mean} = 0.27$ cm^2 V^{-1} s^{-1}). This finding can be basically justified with the presence of residual contact resistance R_C effects which are more relevant at decreasing channel length (L is 100 μm for A, 75 μm for B, and 50 μm for C).[24] On the other hand, devices D, with $L = 50\ \mu$m and $W = 250\ \mu$m, exhibited better results than devices C ($L = 50\ \mu$m and $W = 500\ \mu$m) and comparable performances to devices B. This occurrence seems to suggest that, in this case, the reduction of the overall active area can match better the film crystalline morphology (islands size), and this effect tends to compensate for the detrimental R_C contribution, arising when small channels lengths are involved.

Different from the mobility behavior, the onset voltage V_{on} (see Figure 7b) values did not show any clear dependence on the active channel lengths, and the average values were all comprised between −25 and −33 V. A similar trend can be observed in Figure 7c also for the threshold voltages V_{th}, which mean values ranged between −55 and −61 V. In vacuum, both V_{on} and V_{th} values were found to shift toward less negative voltages approximately by 15 V.

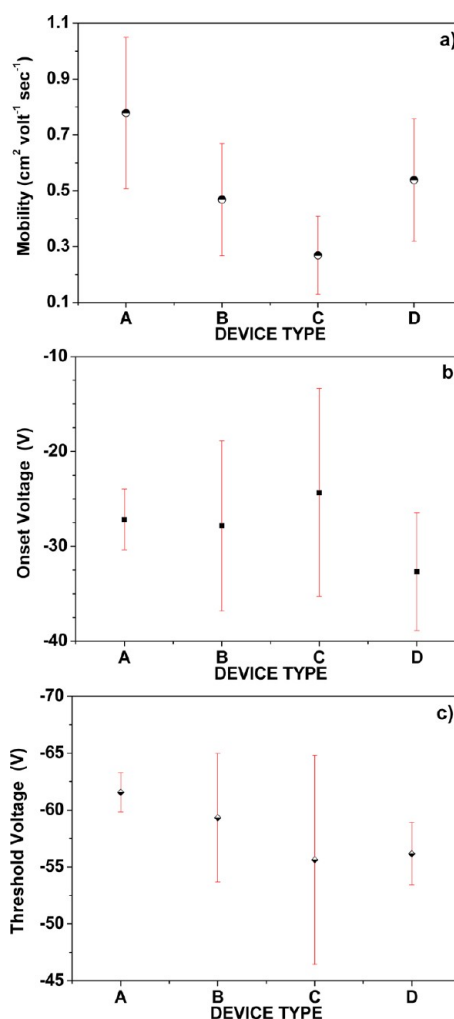The analysis of the electrical response of picene transistors with bottom-contact configuration (with interdigitated source-drain electrodes, as schematically represented in Figure 8a) confirmed the beneficial effect coming from the surface functionalization by HMDS, which, in this case, strongly improves the picene morphology on the gold electrodes. Thus, while we were not able to detect any I_{DS} current exceeding the electrical noise level for bottom-contact devices on bare SiO$_x$/Si substrates, transistors on HMDS-treated surfaces exhibit clear field-effect responses as demonstrated by the transfer curve reported in Figure 8b.

Similar to top-contact devices, hysteresis was large and onset voltages (see the inset of Figure 8b) were close to −20 V. However, the most relevant feature for bottom-contact devices was found for the mobility, which maximum value (we measured about 15 devices) was 2.5×10^{-4} cm^2 V^{-1} s^{-1}. Moreover, only very slight differences between the measurements performed in air and vacuum were found.

The low mobility values measured for the bottom-contact devices, even in presence of a quite ordered morphology (Figure 5b) on the gold electrodes, highlight that the charge injection process from these metal contacts to picene films is ruled by electrical effects which need to be further investigated.
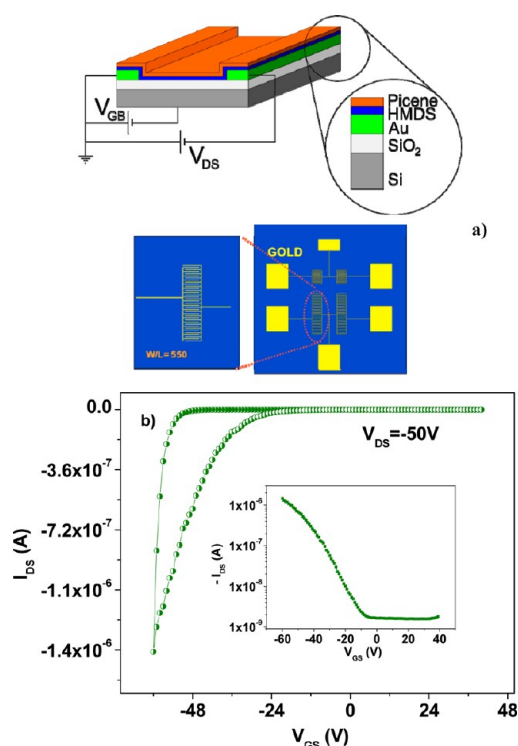
Figure 8. (a) Transistor structure and source-drain interdigitated electrode layout of the bottom-contact devices considered in this work (W = 22 mm, L = 40 μm). (b) Transfer curve in saturation measured in vacuum for a bottom-contact picene transistor.

4. CONCLUSIONS

We investigated the growth of picene thin films deposited by SuMBD on both silicon oxide and self-assembled monolayer of HMDS. The morphology on both surfaces shows well-separated crystalline islands of rather high thickness and very sharp edges. We ascribed this kind of growth to a weak interaction between picene and substrates and a strong interaction among picene molecules. Compared to thermal evaporation techniques, we also observe a larger size of the crystals deposited with SuMBD. This is due to the greater energy available with SuMBD that activates new reaction pathways, such as the direct incorporation of the molecules inside the topmost molecular layer. At the same time surface diffusion is also enhanced. Surfaces play a relevant role in the growth mechanisms and the more hydrophobic character of HMDS with respect to silicon oxide surface leads to a lowered Schwoebel–Ehrlich barrier at the picene–susbtrate interface.

The large size of the crystallites and the tunability of the growth parameters with SuMBD permit to realize devices with optimized characteristics. This was experimentally verified fabricating field-effect transistors on both bare and HMDS-treated SiO_x/Si surfaces. In top-contact devices, HMDS functionalization makes possible a mobility improvement of 3 orders of magnitude with a record value of 1.2 cm^2 V^{-1} s^{-1} measured in air.

The comparison among top-contact transistors with progressively smaller lengths of the active channels, as well as the considerably poor electrical performances measured for bottom-contact devices, demonstrated that the charge injection process from gold electrodes represent a limiting factor for the electrical operation of picene field-effect devices.

AUTHOR INFORMATION

Corresponding Author
*Tel +390461314250; Fax +390461314875; e-mail toccoli@science.unitn.it.

Present Address
#Zernike Institute for Advanced Materials, University of Groningen, Nijenborgh 4, NL-9747 AG Groningen, The Netherlands.

Notes
The authors declare no competing financial interest.

REFERENCES

(1) Okamoto, H.; Kawasaki, N.; Kaji, Y.; Kubozono, Y.; Fujiwara, A.; Yamaji, M. *J. Am. Chem. Soc.* **2008**, *130*, 10470−10471.

(2) Kawasaki, N.; Kubozono, Y.; Okamaoto, H.; Fujiwara, A.; Yamaji, M. *Appl. Phys. Lett.* **2009**, *94*, 043310.

(3) Mitsuhashi, R.; Suzuki, Y.; Yamanari, Y.; Mitamura, H.; Kambe, T.; Ikeda, N.; Okamoto, H.; Fujiwara, A.; Yamaji, M.; Kawasaki, N.; et al. *Nature* **2010**, *464*, 76−79.

(4) Kubozono, Y.; Mitamura, H.; Lee, X.; He, X.; Yamanari, Y.; Takahashi, Y.; Suzuki, Y.; Kaji, Y.; Eguchi, R.; Akaike, K.; et al. *Phys. Chem. Chem. Phys.* **2011**, *13*, 16476−16493.

(5) Wang, X. F.; Yan, Y. J.; Gui, Z.; Liu, R. H.; Yiang, J. J.; Luom, X. G.; Chen, X. H. *Phys. Rev. B* **2011**, *84*, 214523.

(6) Iannotta, S.; Toccoli, T. *J. Polym. Sci., Part B: Polym. Phys.* **2003**, *41*, 2501−2521.

(7) Ruiz, R.; Choudhary, D.; Nickel, B.; Toccoli, T.; Chang, K.; Mayer, A. C.; Clancy, P.; Blakely, J. M.; Headrick, R. L.; Iannotta, S.; et al. *Chem. Mater.* **2004**, *16*, 4497−4508.

(8) Wu, Y.; Toccoli, T.; Koch, N.; Iacob, E.; Pallaoro, A.; Rudolf, P.; Iannotta, S. *Phys. Rev. Lett.* **2007**, *98*, 076601.

(9) Toccoli, T.; Tonezzer, M.; Bettotti, P.; Coppedé, N.; Larcheri, S.; Pallaoro, A.; Pavesi, L.; Iannotta, S. *Org. Electron.* **2009**, *10*, 521−526.

(10) Horcas, I.; Fernandez, R.; Gomez-Rodriguez, J. M.; Colchero, J.; Gomez-Herrero, J.; Baro, A. M. *Rev. Sci. Instrum.* **2007**, *78*, 013705.

(11) Di Girolamo, F. V.; Aruta, C.; Barra, M.; D'Angelo, P.; Cassinese, A. *Appl. Phys. A* **2009**, *96*, 481−487.

(12) Riccio, M.; Irace, A.; Breglio, G.; Rossi, L.; Barra, M.; Di Girolamo, F. V.; Cassinese, A. *Appl. Phys. Lett.* **2008**, *93*, 243504.

(13) Pratontep, S.; Brinkmann, M.; Nuesch, F.; Zuppiroli, L. *Phys. Rev. B* **2004**, *69*, 165201.

(14) Venables, J. A.; Spiller, G. D. T.; Hanbucken, M. *Rep. Prog. Phys.* **1984**, *47*, 399−459.

(15) Dinelli, F.; Moulin, J. F.; Loi, M. A.; Da Como, E.; Massi, M.; Murgia, M.; Muccini, M.; Biscarini, F.; Wie, J.; Kingshott, P. *J. Phys. Chem. B* **2006**, *110*, 258−263.

(16) Kaji, Y.; Kawasaki, N.; Lee, X.; Okamoto, H.; Sugawara, Y.; Oikawa, S.; Ito, A.; Okazaki, H.; Yokoya, T.; Fujiwara, A.; et al. *Appl. Phys. Lett.* **2009**, *95*, 183302.

(17) Goose, J. E.; Killampalli, A.; Clancy, P.; Engstrom, J. R. *J. Phys. Chem. C* **2009**, *113*, 6068−6073.

(18) Schwoebel, R. L.; Shipsey, E. J. *J. Appl. Phys.* **1966**, *37*, 3682−3686.

(19) Schwoebel, R. L. *J. Appl. Phys.* **1969**, *40*, 614−618.

(20) Lee, X.; Sugawara, Y.; Ito, A.; Oikawa, S.; Kawasaki, N.; Kaji, Y.; Mitsuhashi, R.; Okamoto, H.; Fujiwara, A.; Omote, K.; et al. *Org. Electron.* **2010**, *11*, 1394−1398.

(21) Kalb, W. L.; Mathis, T.; Haas, S.; Stassen, A. F.; Batlogg, B. *Appl. Phys. Lett.* **2007**, *90*, 092104−1/3.

(22) Barra, M.; Di Girolamo, F.; Minder, N. A.; Gutierrez Lezama, I.; Chen, Z.; Facchetti, A.; Morpurgo, A. F.; Cassinese, A. *Appl. Phys. Lett.* **2012**, *100*, 133301−1/4.

(23) Kalb, W. L.; Mattenberger, K.; Batlogg, B. *Phys. Rev. B* **2008**, *78*, 035324−1/11.

(24) Bao, Z.; Locklin, J. *Organic Field-Effect Transistors*; Taylor & Francis: Boca Raton, FL, 2007.

24511

dx.doi.org/10.1021/jp304561s | *J. Phys. Chem. C* 2012, 116, 24503−24511